

Dramatic changes in the electronic structure upon transition to the collapsed tetragonal phase in CaFe_2As_2

R. S. Dhaka, Rui Jiang, S. Ran, S. L. Bud'ko, P. C. Canfield, B. N. Harmon, and Adam Kaminski

Ames Laboratory, U.S. DOE and Department of Physics and Astronomy, Iowa State University, Ames, Iowa 50011, USA

Milan Tomić and Roser Valentí

Institut für Theoretische Physik, Goethe-Universität Frankfurt, Max-von-Laue-Straße 1, 60438 Frankfurt am Main, Germany

Yongbin Lee

Ames Laboratory, U.S. DOE, Ames, Iowa 50011, USA

(Received 26 April 2013; revised manuscript received 11 January 2014; published 31 January 2014)

We use angle-resolved photoemission spectroscopy and density functional theory calculations to study the electronic structure of CaFe_2As_2 in the collapsed tetragonal (CT) phase. This unusual phase of iron arsenic high-temperature superconductors was hard to measure as it exists only under pressure. By inducing internal strain, via the postgrowth thermal treatment of single crystals, we were able to stabilize the CT phase at ambient pressure. We find significant differences in the Fermi surface topology and band dispersion data from the more common orthorhombic-antiferromagnetic or tetragonal-paramagnetic phases, consistent with electronic structure calculations. The top of the hole bands sinks below the Fermi level, which destroys the nesting present in parent phases. The absence of nesting in this phase, along with an apparent loss of Fe magnetic moment, are now clearly experimentally correlated with the lack of superconductivity in this phase.

DOI: [10.1103/PhysRevB.89.020511](https://doi.org/10.1103/PhysRevB.89.020511)

PACS number(s): 74.25.Jb, 74.62.Dh, 74.70.-b, 79.60.-i

The AFe_2As_2 ($A = \text{Ca, Sr, Ba}$) materials have become one of the key systems for the study of Fe-based high-temperature superconductivity [1–10]. Detailed substitution and pressure studies on these systems have revealed that superconductivity is intimately linked to the magnetic state of iron and can be turned on or off by manipulating the nature of the order, the fluctuations, or even the existence of Fe magnetism [6–15]. Moreover, in contrast to cuprate superconductors, the Fe-based superconductors are multiorbital systems and orbital degrees of freedom have been also proposed to be important for the understanding of the structural, magnetic, and superconducting properties of these materials [16–18]. At ambient pressure CaFe_2As_2 manifests a strongly first-order, coupled structural-magnetic phase transition at 170 K that is exceptionally pressure sensitive with a remarkably large pressure derivative [9,10]. For pressures as low as 0.4 GPa, another dramatic, first-order phase transition to a nonmoment bearing collapsed tetragonal (CT) phase [9] is stabilized near 100 K and rapidly increases in temperature for higher applied pressures. Whereas the electronic properties of CaFe_2As_2 in the ambient pressure phases [19,20] were found to be similar to the other parent compounds of the 122 family [21–28], the electronic behavior of the CT phase is so far largely unexplored due to the need for at least 0.4 GPa of external pressure.

Postgrowth annealing and quenching of CaFe_2As_2 samples grown from excess FeAs can be used to control the degree of internal strain due to Fe-As precipitates associated with a small width of formation [29–31]. One of the important findings of these works is that the nonmagnetic, collapsed tetragonal phase can be stabilized in an ambient pressure sample by using internal strain. Key spectroscopic tools, such as angle-resolved photoemission spectroscopy (ARPES) and scanning tunneling microscopy (STM), which normally cannot be combined with pressures even at the 0.1 GPa level, can now be brought into

play in order to understand the electronic properties of the collapsed tetragonal phase.

In this Rapid Communication we present ARPES measurements of the electronic properties of CaFe_2As_2 in the CT phase and compare them with the orthorhombic and (noncollapsed) tetragonal phases. Our data demonstrate that the band dispersion and Fermi surface (FS) topology change significantly with the transition to the CT phase, in agreement with our electronic structure calculations. In particular, the tops of the bands associated with Fe d_{xy} and $d_{xz} + d_{yz}$ states at the center of the Brillouin zone move from above E_F to just below E_F , eliminating the hole pockets. Whereas there are significant changes elsewhere (to maintain electron count), loss of the nesting between the hole and electron sheets brought about by the shifts we observe are of key importance for magnetic and superconducting states in the low pressure phase [32]. Our findings provide a peek into a phase that was previously accessible only under external pressure and provide further evidence of an intimate relation between the nature and nesting of the Fermi surface and magnetism in the iron arsenic high-temperature superconductors.

Single crystals of CaFe_2As_2 were grown from excess FeAs by slowly cooling a melt of CaFe_4As_4 from 1180 to 960 °C and then decanting off the excess liquid, essentially quenching the samples from 960 °C to room temperature, which is referred to as the “960C” sample [29]. Upon cooling, this sample becomes nonmagnetic and has a CT unit cell with a significantly reduced c/a ratio for $T \lesssim 100$ K. This is remarkably similar to what has been observed for Sn grown CaFe_2As_2 samples under hydrostatic pressure (0.6 GPa) [29]. Postgrowth thermal treatments of these samples involve annealing at temperatures ranging from 350 to 800 °C for 24 h, and subsequently quenching them from this annealing temperature to room temperature. Here, we have measured three samples

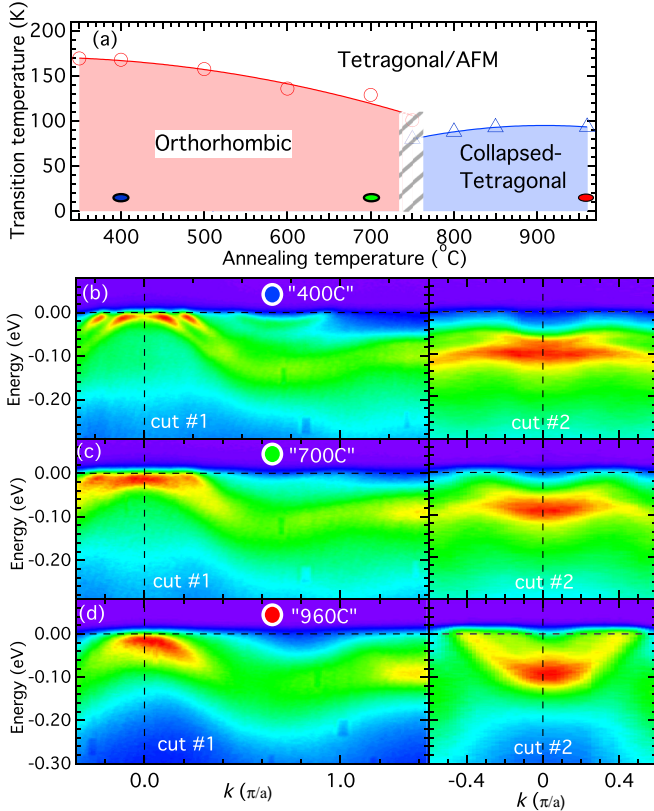


FIG. 1. (Color online) (a) Schematic phase diagram for the CaFe_2As_2 system based on data in Ref. [29]. Blue, green, and red circles mark the annealing condition of samples used in this study. The hatched area marks the boundary between two distinct phases. (b)–(d) Band dispersion along cuts No. 1 and No. 2 for the three samples measured at $T = 15$ K and $k_z = 15.3\pi/c$.

identified by their annealing and quenching temperatures: “400C,” “700C,” and “960C.” As shown in Fig. 1(a), these three samples cover the salient parts of the phase diagram: the ~ 170 K transition to low-temperature antiferromagnetic (AFM)-orthorhombic (“400C”), the ~ 120 K transition to AFM-orthorhombic (“700C”), and the ~ 100 K transition to the nonmagnetic CT phase (“960C”). At ambient conditions, the properties of the last two samples are remarkably similar to ones where hydrostatic pressure is applied to Sn grown samples of 0.35 and 0.675 GPa [10,29]. ARPES measurements have been performed [in grazing incidence geometry shown in Fig. 1(v) of Ref. [33]] at beamline 10.0.1 of the Advanced Light Source (ALS) using a Scienta R4000 electron analyzer. The measurements at Ames Laboratory were acquired using a Scienta SES2002 electron analyzer and a GammaData helium ultraviolet lamp. The samples were mounted on an Al pin using UHV compatible epoxy and *in situ* cleaved perpendicular to the c axis, yielding single layer surfaces in the a - b plane. All ARPES data were collected in ultrahigh vacuum with pressures better than 4×10^{-11} Torr. The energy and angular resolutions were set at ≈ 15 meV and $\approx 0.3^\circ$, respectively. The Fermi level (E_F) of the samples was referenced by measuring for a Au film evaporated *in situ* onto the sample holder. High symmetry points were defined in the same way as in Ref. [34]. The measurements carried out on several samples yielded

similar results for the band dispersion and FSs. *Ab initio* calculations [35,36] based on density functional theory (DFT) as implemented in the Vienna *ab initio* simulation package (VASP), [37] combined with the fast inertial relaxation engine (FIRE) algorithm [38], were performed at finite pressure, both for compressive and tensile stress. A collapsed tetragonal phase was obtained in the calculations only for isotropically applied pressures as well as uniaxial pressures along the c axis.

The evolution of the band structure with annealing and quenching temperature, which is equivalent to applying pressure, for $k_z = 15.3\pi/c$, is shown in Fig. 1. Because there is a significant decrease in the c -axis lattice parameter in the CT phase, we used different photon energies in order to compare data at similar values of k_z . This momentum plane was selected for the best signal-to-background ratio and clarity of the band dispersion in data (matrix elements). This momentum plane is accessed using 45 eV photons for the orthorhombic-tetragonal phases and 62 eV for the CT phase. Figures 1(b)–1(d) show the band dispersion along two cuts [marked in Fig. 2(a)] for the “400C,” “700C,” and “960C” samples, respectively. The first two samples remain in the orthorhombic-antiferromagnetic phase at low temperatures. At this value of k_z and $T = 15$ K, the matrix elements and relatively low scattering allow for the observation of two well separated hole bands in the “400C” sample. These bands broaden in the “700C” sample, most likely due to some degree of inhomogeneous stress being present. The “960C” sample at low temperature is in the CT phase, which is equivalent to an application of 0.7 GPa of hydrostatic pressure to stress-free, Sn flux grown samples [10,29,30]. The band structure in this phase is very different indeed, as illustrated in Fig. 1(d). The hole pockets sink below the Fermi energy while the electron band moves to a higher binding energy and becomes more dispersive and sharper. The vanishing of large portions of the hole Fermi sheets in the CT phase resembles to a degree the situation in its structural analog, CaFe_2P_2 [39].

In Fig. 2 we plot the Fermi surface and band dispersion in all three phases that occur in the CaFe_2As_2 . The tetragonal-paramagnetic phase can be accessed at higher temperatures in both the “400C” and “960C” samples [see the phase diagram in Fig. 1(a)]. The data in the orthorhombic and tetragonal phases was measured using 35 eV, which corresponds to $k_z = 13.5\pi/c$. The same value of k_z is accessed in the CT phase when using 45 eV photons. The Fermi surface maps for these phases are shown in Figs. 2(a) and 2(g) and the band dispersions along two symmetry cuts are shown in Figs. 2(b) and 2(c) and Figs. 2(h) and 2(i) for the “400C” and “960C” samples, respectively. The electronic structure of the tetragonal phase consists of two hole pockets at the center of the zone and two electron pockets at the corners of the zone. Due to increased scattering at high temperatures, the pairs of bands appear as a single, broader streak of intensity. These high-temperature data are very similar to data measured in parent compounds in the 122 family at ambient pressures [19,33,40]. The “400C” sample has similar properties to samples at ambient pressure [29], e.g., grown using Sn flux that is stress free [see the phase diagram in Fig. 1(a)]. Upon cooling, the “400C” sample enters the well documented orthorhombic-antiferromagnetic phase. This is evident from

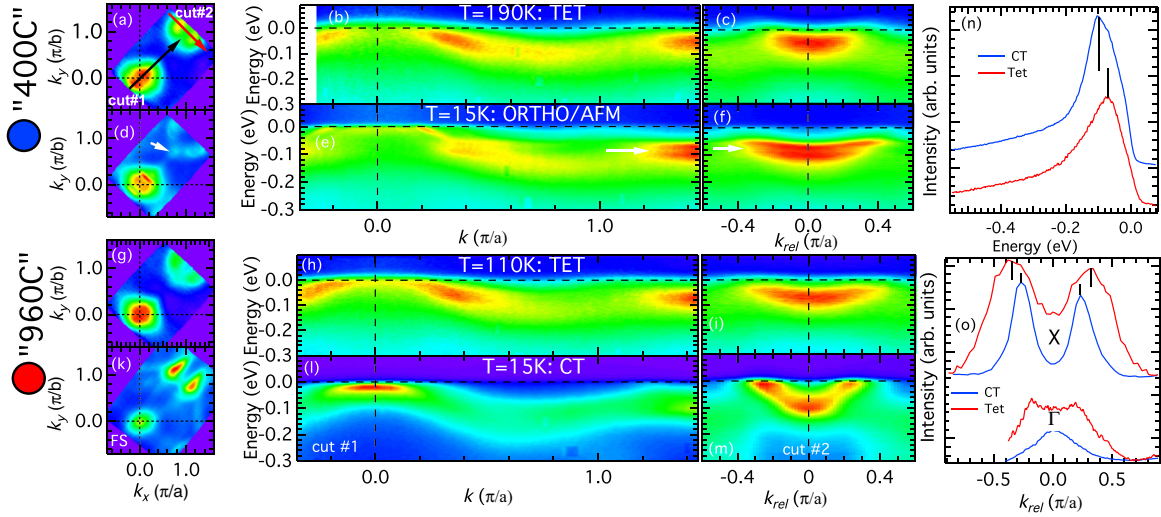


FIG. 2. (Color online) The band structure of CaFe_2As_2 in three different phases measured at $k_z = 13.5\pi/c$. (a) Fermi surface map. (b) Band dispersion along cut No. 1 [marked in (a)]. (c) Band dispersion along cut No. 2 measured at 190 K in the tetragonal-paramagnetic phase for a sample that was postgrowth annealed at 400 °C. (d)–(f) The same plots for the same sample measured at 15 K in the orthorhombic-antiferromagnetic phase. The arrow in (d) points to small pockets associated with AFM order, while arrows in (e) and (f) point to band splitting caused by AFM order. (g)–(i) The same plots for a sample that was postgrowth annealed at 960 °C measured at 110 K again in the tetragonal-paramagnetic phase. (k)–(m) The same plots for the “960C” sample, but measured at $T = 15$ K in the CT phase. (n) EDCs at the corner of the zone, $k = (1, 1)$. The location of the peak marks the energy of the bottom of the electron pocket. (o) MDCs at the center of the zone (the bottom two curves) and the corner of the zone (the top two curves).

data in Figs. 2(d)–2(f), where complicated Fermi surface reconstruction (straight, nested sections of the hole pockets and sharp, high intensity points in electron pockets) and splitting of the bands at high energy are present. This is fully consistent with previous data in the AFM state [19,20,22,28,41,42] and

signifies that “400C” samples are indeed ambient and low pressure equivalent.

As previously mentioned, the “960C” sample shows a transition from the high-temperature tetragonal phase [Figs. 2(g)–2(i)] to the CT phase [Figs. 2(k)–2(m)] upon cooling. Overall,

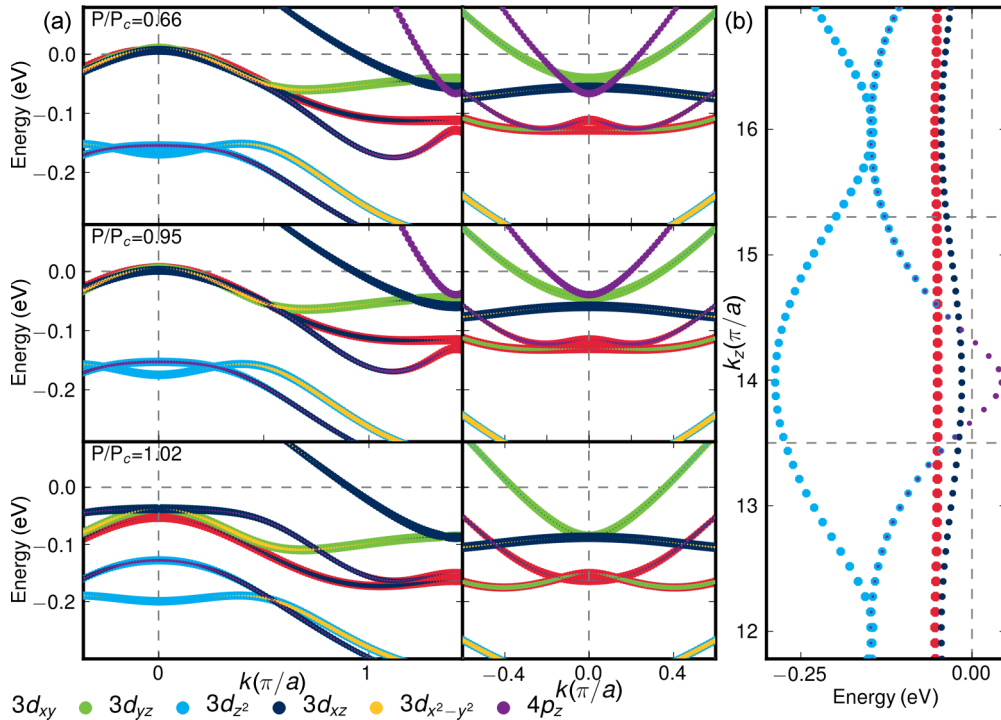


FIG. 3. (Color online) Results of the DFT calculation of the band structure in CT at $k_z = 15.3\pi/c$ corresponding to ARPES data shown in Fig. 1. (a) The left column shows band dispersion at the zone center, and the right column corresponds to the zone corner. (b) Calculated band dispersion along the k_z direction. Dashed lines mark the k_z values of data in Figs. 1 and 2. Colors denote orbital contributions.

the band dispersion in the CT phase at this k_z plane [Figs. 2(l) and 2(m)] is very similar to the data in Fig. 1. The appearance of brighter spots at different [from data in Fig. 1(d)] momentum points for both hole and electron bands signifies modifications in the matrix elements due to the different photon energies used. Overall, the electronic properties in the CT phase agree qualitatively with the recently reported theoretical calculations [35,36,43]. Perhaps the most striking characteristic of the CT phase is the sinking of the hole pockets under the E_F and associated with this lack of the Fermi surface nesting. We quantify the key changes in the band dispersion by plotting the energy distribution curves (EDCs) and momentum distribution curves (MDCs) at the high symmetry points in Figs. 2(n) and 2(o). In the CT phase, the bottom of the electron pocket moves to a higher binding energy from ~ 70 to ~ 90 meV, as shown in Fig. 2(n). At the same time the diameter of the electron pocket shrinks slightly and the MDC peaks become sharper [the top two curves in Fig. 2(o)]. The MDCs close to the zone center have two peaks in the tetragonal phase, which signifies the presence of a finite size hole pocket. Upon transition to the CT phase only a weaker, single peak centered at the (0,0) is present [the lower curve in Fig. 2(o)], which is consistent with an absence of the hole pocket at this k_z plane and the top of this band being located below the chemical potential.

Results of the DFT calculations of the band structure across the orthorhombic-CT phase transition are shown in Fig. 3. We observe that simulations under hydrostatic pressure mimic ARPES data most closely, when renormalization by a factor of 5 is employed [44]. In particular, we find close correspondence between the observed Fermi surface behavior of the “700C” and “960C” structures and $P/P_c = 0.95$, and $P/P_c = 1.02$ hydrostatic pressure structures, in the immediate vicinity of the orthorhombic-to-CT phase transition at P_c . At the transition, the d_{xy} , d_{yz} , and d_{xz} bands abruptly drop below the Fermi level around the Γ point, causing hole cylinders parallel to the k_z axis to quickly disappear completely within the collapsed tetragonal phase, as observed in the ARPES measurements. These changes in the electronic structure show clearly that the tetragonal-CT and orthorhombic-CT phase transitions cannot be explained through a rigid band shift, as has been also discussed in Co-doped Ca122 [45]. In Fig. 3(b) we plot the calculated band dispersion in the CT phase along the z direction at the center of the zone. Except for a very small crossing at E_F by one of the bands around $k_z = 14\pi/c$, most of the bands are located below the chemical potential.

To examine the electronic properties along the z direction and ensure that the differences we reported in the CT phase do not arise due to some unforeseen complications related to k_z dispersion, we measured the FS and band structure using a wide range of photon energies. The FS maps for selected photon energies are shown in Figs. 4(a)–4(d). There is very little variation in the overall shape of the Fermi surface. The intensity of the inner and outer electron pockets changes with photon energy due to the matrix elements, but their separation remains almost constant. Intensity plots along cut No. 1 in the CT phase measured using several photon energies are shown in Fig. 4(e). The top of the band at the center of the zone appears to be consistently located below the chemical potential and

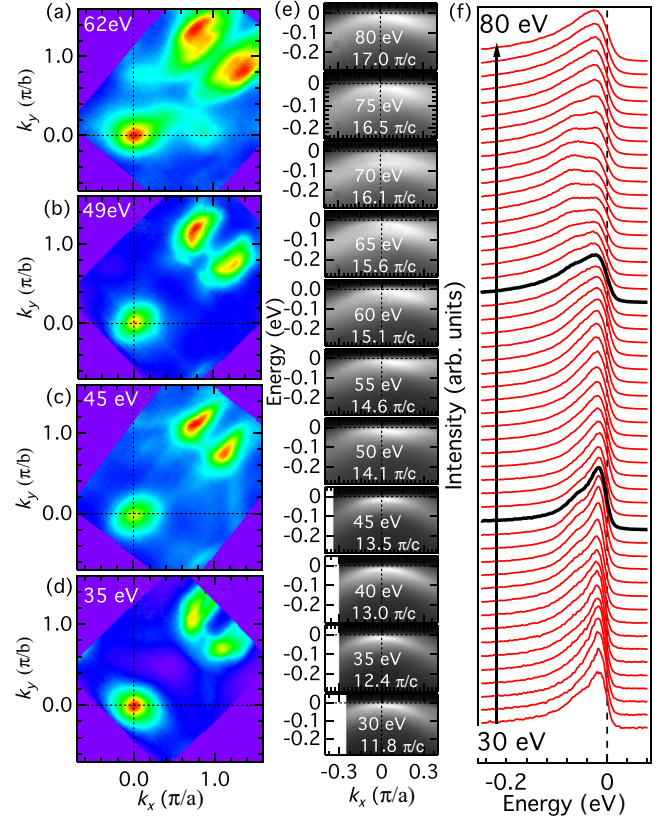


FIG. 4. (Color online) FS maps of the CaFe_2As_2 “960C” sample measured with (a) 35, (b) 45, (c) 49, and (d) 62 eV photon energies at $T_S \approx 15$ K. (e) Intensity plots close to the center of the zone along cut No. 1 for photon energies from 30 to 80 eV. (f) EDCs at the center of the zone for photon energies from 30 to 80 eV, plotted every 1 eV. Thick (black) lines mark photon energies of 45 and 62 eV used in Figs. 1 and 2.

the crossing predicted by the calculations [see Fig. 3(b)] is not directly visible in the data. This could be due to the matrix elements, or an overwhelming intensity from the broad bands located below E_F . In Fig. 4(f) we plot EDC curves at the zone center as a function of photon energy with 1 eV steps. In addition to a sharp peak just below E_F , a second peak at a higher binding energy can be observed for a range of k_z values centered at $\sim 12.5\pi/c$ and $\sim 16\pi/c$. These structures most likely correspond to the overlap of the d_{xz} and d_{z^2} bands shown in Fig. 3(b). Based on the DFT calculation, one would expect two broader, main peaks at binding energies of -50 and -150 meV, while those peaks are observed in the data at -18 and -68 meV. This discrepancy can be attributed to correlation effects which are not properly accounted for in the DFT calculations. These effects can lead to strong band renormalizations [46,47]. The Fermi crossing around $k_z = 14\pi/c$ is not directly seen in the data, most likely due to the relatively weak intensity of this band.

In conclusion, our results reveal the electronic structure of the CT phase in unsubstituted CaFe_2As_2 . Our data demonstrate that the FS and band dispersion in the CT phase are significantly different from ambient pressure phases and are in qualitative agreement with theoretical calculations for this phase. The hole pockets do not extend over an

appreciable range of k_z values and the destruction of nesting is accompanied by the vanishing of Fe magnetic moments and order. The resulting lack of magnetic fluctuations could be responsible for the absence of superconductivity in this phase.

Note added. Recently we became aware of a study of the electronic structure of the CT phase in chemically substituted $\text{Ca}(\text{Fe}_{1-x}\text{Rh}_x)_2\text{As}_2$ by Tsubota *et al.* [48].

We thank Sung-Kwan Mo for instrumentation support at the ALS. This work was supported by the U.S. Department

of Energy (DOE), Office of Science, Basic Energy Sciences, Materials Science and Engineering Division. Ames Laboratory is operated for the U.S. DOE by Iowa State University under contract No. DE-AC02-07CH11358 (sample growth, ARPES measurements, and data analysis). M.T. and R.V. thank the Deutsche Forschungsgemeinschaft for funding through Grant No. SPP 1458 (DFT calculations). The Advanced Light Source is supported by the Director, Office of Science, Office of Basic Energy Sciences, of the U.S. Department of Energy under Contract No. DE-AC02-05CH11231.

-
- [1] Y. Kamihara, T. Watanabe, M. Hirano, and H. Hosono, *J. Am. Chem. Soc.* **2130**, 3296 (2008).
 - [2] H. Takahashi, K. Igawa, K. Arii, Y. Kamihara, M. Hirano, and H. Hosono, *Nature (London)* **453**, 376 (2008).
 - [3] X. H. Chen, T. Wu, G. Wu, R. H. Liu, H. Chen, and D. F. Fang, *Nature (London)* **453**, 761 (2008).
 - [4] T. Y. Chen, Z. Tesanovic, R. H. Liu, X. H. Chen, and C. L. Chien, *Nature (London)* **453**, 1224 (2008).
 - [5] G. F. Chen, Z. Li, D. Wu, G. Li, W. Z. Hu, J. Dong, P. Zheng, J. L. Luo, and N. L. Wang, *Phys. Rev. Lett.* **100**, 247002 (2008).
 - [6] M. Rotter, M. Tegel, and D. Johrendt, *Phys. Rev. Lett.* **101**, 107006 (2008).
 - [7] C. de la Cruz *et al.*, *Nature (London)* **453**, 899 (2008).
 - [8] A. S. Sefat, R. Jin, M. A. McGuire, B. C. Sales, D. J. Singh, and D. Mandrus, *Phys. Rev. Lett.* **101**, 117004 (2008).
 - [9] N. Ni, S. Nandi, A. Kreyssig, A. I. Goldman, E. D. Mun, S. L. Bud'ko, and P. C. Canfield, *Phys. Rev. B* **78**, 014523 (2008).
 - [10] P. C. Canfield, S. L. Bud'ko, N. Ni, A. Kreyssig, A. I. Goldman, R. J. McQueeney, M. S. Torikachvili, D. N. Argyriou, G. Luke, and W. Yu, *Physica C* **469**, 404 (2009).
 - [11] D. C. Johnston, *Adv. Phys.* **59**, 803 (2010).
 - [12] P. C. Canfield and S. L. Bud'ko, *Annu. Rev. Condens. Matter Phys.* **1**, 27 (2010).
 - [13] P. J. Hirschfeld, M. M. Korshunov, and I. I. Mazin, *Rep. Prog. Phys.* **74**, 124508 (2011).
 - [14] H. Lee, E. Park, T. Park, V. A. Sidorov, F. Ronning, E. D. Bauer, and J. D. Thompson, *Phys. Rev. B* **80**, 024519 (2009).
 - [15] P. L. Alireza, Y. T. C. Ko, J. Gillett, C. M. Petrone, J. M. Cole, G. G. Lonzarich, and S. E. Sebastian, *J. Phys.: Condens. Matter* **21**, 012208 (2008).
 - [16] F. Kruger, S. Kumar, J. Zaanen, and J. van den Brink, *Phys. Rev. B* **79**, 054504 (2009).
 - [17] C.-C. Lee, W.-G. Yin, and W. Ku, *Phys. Rev. Lett.* **103**, 267001 (2009).
 - [18] W.-C. Lee, J. M. Tranquada, and P. W. Phillips, *Phys. Rev. B* **86**, 094516 (2012) and references therein.
 - [19] C. Liu *et al.*, *Phys. Rev. Lett.* **102**, 167004 (2009).
 - [20] T. Kondo *et al.*, *Phys. Rev. B* **81**, 060507(R) (2010).
 - [21] T. Shimojima *et al.*, *Phys. Rev. Lett.* **104**, 057002 (2010).
 - [22] L. X. Yang *et al.*, *Phys. Rev. Lett.* **102**, 107002 (2009).
 - [23] T. Sato *et al.*, *Phys. Rev. Lett.* **103**, 047002 (2009).
 - [24] J. Fink *et al.*, *Phys. Rev. B* **79**, 155118 (2009).
 - [25] M. Fuglsang Jensen, V. Brouet, E. Papalazarou, A. Nicolaou, A. Taleb-Ibrahimi, P. Le Fèvre, F. Bertran, A. Forget, and D. Colson, *Phys. Rev. B* **84**, 014509 (2011).
 - [26] G. Liu *et al.*, *Phys. Rev. B* **80**, 134519 (2009).
 - [27] B. Zhou *et al.*, *Phys. Rev. B* **81**, 155124 (2010).
 - [28] M. Yi *et al.*, *Phys. Rev. B* **80**, 174510 (2009); **80**, 024515 (2009).
 - [29] S. Ran *et al.*, *Phys. Rev. B* **83**, 144517 (2011).
 - [30] S. Ran, S. L. Bud'ko, W. E. Straszheim, J. Soh, M. G. Kim, A. Kreyssig, A. I. Goldman, and P. C. Canfield, *Phys. Rev. B* **85**, 224528 (2012).
 - [31] E. Gati, S. Köhler, D. Guterding, B. Wolf, S. Knöner, S. Ran, S. L. Bud'ko, P. C. Canfield, and M. Lang, *Phys. Rev. B* **86**, 220511 (2012).
 - [32] R. S. Dhaka, S. E. Hahn, E. Razzoli, R. Jiang, M. Shi, B. N. Harmon, A. Thaler, S. L. Bud'ko, P. C. Canfield, and A. Kaminski, *Phys. Rev. Lett.* **110**, 067002 (2013).
 - [33] R. S. Dhaka *et al.*, *Phys. Rev. Lett.* **107**, 267002 (2011).
 - [34] C. Liu *et al.*, *Nat. Phys.* **6**, 419 (2010); *Phys. Rev. B* **84**, 020509(R) (2011).
 - [35] M. Tomić, R. Valentí, and H. O. Jeschke, *Phys. Rev. B* **85**, 094105 (2012).
 - [36] M. Tomić, H. O. Jeschke, R. M. Fernandes, and R. Valentí, *Phys. Rev. B* **87**, 174503 (2013).
 - [37] G. Kresse and J. Hafner, *Phys. Rev. B* **47**, 558 (1993); G. Kresse and J. Furthmüller, *ibid.* **54**, 11169 (1996); *Comput. Mater. Sci.* **6**, 15 (1996).
 - [38] E. Bitzek, P. Koskinen, F. Gähler, M. Moseler, and P. Gumbsch, *Phys. Rev. Lett.* **97**, 170201 (2006).
 - [39] A. I. Coldea, C. M. J. Andrew, J. G. Analytis, R. D. McDonald, A. F. Bangura, J.-H. Chu, I. R. Fisher, and A. Carrington, *Phys. Rev. Lett.* **103**, 026404 (2009).
 - [40] P. Vilmercati *et al.*, *Phys. Rev. B* **79**, 220503(R) (2009).
 - [41] G. Liu *et al.*, *Phys. Rev. B* **80**, 134519 (2009).
 - [42] Y. Zhang *et al.*, *Phys. Rev. Lett.* **102**, 127003 (2009).
 - [43] A. Sanna, G. Profeta, S. Massidda, and E. K. U. Gross, *Phys. Rev. B* **86**, 014507 (2012).
 - [44] The fact that bands have to be renormalized by a factor of 5 indicates that the effects of correlations are important in this system under various pressure conditions.
 - [45] G. Levy *et al.*, *Phys. Rev. Lett.* **109**, 077001 (2012).
 - [46] Z. P. Yin, K. Haule, and G. Kotliar, *Nat. Mater.* **10**, 932 (2011).
 - [47] J. Ferber, H. O. Jeschke, and R. Valentí, *Phys. Rev. Lett.* **109**, 236403 (2012).
 - [48] K. Tsubota *et al.*, *J. Phys. Soc. Jpn.* **82**, 073705 (2013).